# Correlation-adaptive Multi-view CEUS Fusion for Liver Cancer Diagnosis

Peng Wan[1][0000−0002−6094−7250], Shukang Zhang[1], Wei Shao[1], Junyong Zhao[1], Yinkai Yang[1], Wentao Kong[2], Haiyan Xue[2], and Daoqiang Zhang[1]

[1] College of Artificial Intelligence, Nanjing University of Aeronautics and Astronautics, Key Laboratory of Brain-Machine Intelligence Technology, Ministry of Education, Nanjing 211106, China.
dqzhang@nuaa.edu.cn

[2] Department of Ultrasound, Nanjing Drum Tower Hospital, Affiliated Hospital of Medical School, Nanjing University, Nanjing 210002, China
xhainiao@163.com

**Abstract.** Dual-screen contrast-enhanced ultrasound (CEUS) has been the first-line imaging techniques for the differential diagnosis of primary liver cancer (PLC), since the imaging of tumor micro-circulation perfusion as well as anatomic features of B-mode ultrasound (BUS) view. Although previous multi-view learning methods have shown their potential to boost diagnostic efficacy, correlation variances of different views among subjects are largely underestimated, arising from the varying imaging quality of different views and the presence of valuable findings or not. In this paper, we propose a correlation-adaptive multi-view fusion method (CAMVF) for dual-screen CEUS based PLC diagnosis. Towards a reliable fusion of multi-view CEUS findings (i.e., BUS, CEUS and its parametric imaging), our method dynamically assesses the correlation of each view based on the prediction confidence itself and prediction consistency among views. Specifically, we first obtain the confidence of each view with evidence-based uncertainty estimation, then divide them into credible and incredible views based on cross-view consistency, and finally ensemble views with weights adaptive to their credibility. In this retrospective study, we collected CEUS imaging from 238 liver cancer patients in total, and our method achieves the superior diagnostic accuracy and specificity of 88.33% and 92.48%, respectively, demonstrating its efficacy for PLC differential diagnosis. Our code is available at https://github.com/shukangzh/CAMVF

**Keywords:** Multi-view fusion · Contrast-enhanced ultrasound · Liver Cancer Diagnosis.

## 1 Introduction

Primary liver cancer (PLC) ranks as the fourth leading cause of cancer-related death worldwide, posing a major threat to public health[17]. Hepatocellular carcinoma (HCC) and intrahepatic cholangiocarcinoma (ICC) are the two major

subtypes of PLC, which differ notably in genetic alteration, molecular patterns, and treatment selection, etc[6]. Taking hepatectomy as example, ICC generally requires a larger surgical resection margin than that of HCC since ICC is more aggressive[18]. Therefore, an accurate differential diagnosis of HCC and ICC is important to therapeutic planning and improve patient prognosis. Dual-screen contrast-enhanced ultrasound (CEUS) stands as the principle imaging techniques for liver cancer differential diagnosis[5], where B-mode ultrasound (BUS) and CEUS are displayed side by side. The two US views provide tumor morphologic findings (i.e., shape, size, margin, echo, etc.) and microvascular perfusion characteristics, respectively. For CEUS view, diverse enhancement patterns are associated with tumor pathological characteristics (i.e., microvessel distribution, tissue necrosis, and the degree of peripheral invasion, etc.)[12], functioning as an important complementary imaging to conventional BUS in clinics[4]. According to the arrival time of contrast agents, the whole liver perfusion examination is split into three phases, i.e., arterial phase, portal phase, and delayed phase. In practice, radiologists generally observe contrast enhancement patterns within different phases and perform a comprehensive evaluation of tumor perfusion for disease diagnosis.

Recently, multi-view learning and attention-based temporal fusion methods achieve state-of-the-art performances in CEUS analysis[9,8,7], which integrates morphological features from BUS view and multi-phase perfusion features from CEUS view for follow-up tasks. However, these methods largely underestimate correlation variances of different views for each subject, susceptible to the noisy or irrelevant views. On the one hand, there exist low-quality ultrasound images corrupted by imaging noise or unpredictable liver motion. On the other hand, there exist less-correlated views without presence of valuable perfusion characteristics for PLC diagnosis. That is, the imaging quality and correlation may vary for different views among patients due to uncertain factors, including acquisition equipment, operator's experiences, and patient disease progression stage, etc. Traditional methods usually presume upon a stable view quality or importance for all samples, and assign equal or fixed weights for view fusion[3,15,7,8]. It is inapplicable to multi-view CEUS fusion for the high-risk liver cancer aided diagnosis, and their frequently biased predictions result in a limited practical deployment value.

In this paper, we propose a correlation-adaptive multi-view fusion method (CAMVF) to assist PLC differential diagnosis using multi-view CEUS. To be adaptive to dynamically changing CEUS view correlation, as shown in Fig 1, our CAMVF method introduces Dempster-Shafer evidence theory (DST)[16] to measure the uncertainty of each view. Compared with other metric of uncertainty, DST theory models prediction uncertainty using beliefs from different views obtained by replacing the Softmax operator with a non-negative activation (ReLU)[20]. For the application of liver cancer aided diagnosis, DST metric of view uncertainty is significantly more feasible due to its substantially reduced computational complexity. The term "**correlation**" in our CAMVF method refers to the degree to which each view contributes to the final decision, de-

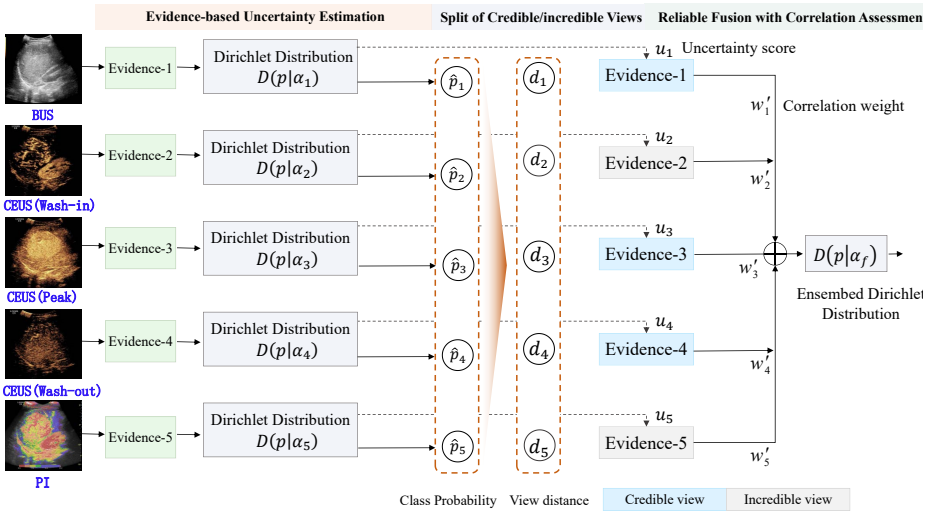


**Fig. 1.** The framework of the proposed correlation-adaptive multi-view fusion (CAMVF) method, which consists of evidence-based uncertainty estimation, split of credible/incredible Views and reliable fusion with correlation assessment.

termined by the confidence of view itself and consistency among views simultaneously. The most relevant work to our CAMVF method is uncertainty-aware trusted multi-view classification (TMC)[10,14] that combines view evidences in terms of Dempster's rule. But Dempster's rule probably produce counter-intuitive results when dealing with highly conflicting evidence[11]. Due to the incremental combination procedure, the combined result may be biased by one view that contradicts with the previous result with a high confidence, and the overall uncertainty increases accordingly. To overcome this limitation, we propose to first divide all views into credible and incredible ones based on cross-view semantic consistency, and then assess their correlation weights by the introduced reward and penalty function, respectively. For the credible view supported by others, the higher view confidence deserves a larger weight for view combination, while for the incredible view conflicting with others, the higher confidence results in a lower fusion weight. In this way, we expect to construct a reliable multi-view CEUS fusion mechanism against inter-view correlation variance for PLC diagnosis.

## 2 Materials and Method

### 2.1 Datasets and Image Pre-Processing

In this study, we totally collected 238 dual-view CEUS cine-loops from patients who attended Nanjing Drum Tower Hospital for liver cancer examination. 136 hepatocellular carcinoma (HCC) and 102 intrahepatic cholangiocarcinoma (ICC)

cases were included. The size of lesion is 35.8cm$^2$ and 43.32cm$^2$ for HCC and ICC, respectively. Pathologies of all cases were determined based on biopsy or surgical specimens. All examinations were performed on a Logiq E9 ultrasound scanner(GE Healthcare, Milwaukee, WI, USA) with a low mechanical index below 0.15. For multi-view CEUS fusion model evaluation, we collected images from five CEUS views for each subject, including the synchronous B-mode ultrasound (BUS), 3 CEUS frames from different perfusion phases, as well as one parametric image (PI) of contrast arrival time generated from Philips iU22 scanner.

To obtain the appropriate CEUS frames, we first perform liver motion compensation by tracking liver tissues with feature descriptors (compact and real-time descriptors, CARD), and then extract CEUS frames from the perfusion peak point as well as the points at which perfusion intensity achieves the 50% peak value both from wash-in and wash-out stages. The spatial resolution of cropped US views are about 780×530. Considering the limited CEUS data, we follow the guidelines of Image Biomarker Standardization Initiative (IBSI)[21] for feature extraction. For BUS view, we extract 146-dimensional features, covering size, shape, orientation, margin, internal echoes, and posterior echoes, etc. For CEUS view, we extract 152-dimensional features, including first-order and high-order echo texture features, as well as differences of tumor regions and their adjacent tissues. For PI view, we extract 49-dimensional statistic features to describe the heterogeneous distribution of contrast initial arrival time.

### 2.2 Correlation-driven Multi-view Fusion

For high-stakes liver cancer diagnosis application, our focus extends beyond the mere identification of disease type. It is imperative to interpret CEUS view fusion decision process, including which views contribute most to the final decision and the level of prediction confidence. To this end, we introduce evidence-based uncertainty (EvU) estimation under the Dempster-Shafer evidence theory. With uncertainty assessment, we expect to identify credible views for reliable multi-view CEUS fusion.

**Problem Formulation** The overall architecture of the proposed correlation-adaptive multi-view fusion (CAMVF) method is illustrated in Fig. 1. Given multi-view CEUS data $\left\{\left(\mathrm{I}_i^{US}, \mathrm{I}_i^{CEUS}, \mathrm{I}_i^{PI}\right), y_i\right\}_{i=1}^{N}$, where $\mathrm{I}_i^{US}$, $\mathrm{I}_i^{CEUS}$ and $\mathrm{I}_i^{PI}$ denote BUS view, CEUS view and parametric view, respectively. Note that, $\mathrm{I}_i^{CEUS}$ contains three CEUS frames from different perfusion stages. The objective of this method is to access the correlation of each view dynamically and fuse them with adaptive weights, achieving a reliable fusion of views for liver cancer type prediction $y_i$.

**Evidence-based Uncertainty Estimation (EvU)** Formally, Dempster-Shafer theory (DST) models the distribution of each set of class probability $\mathbf{p}$ with the variational Dirichlet, parameterized with class-wise evidence collected from input

view. For K-classification problem, Dirichlet distribution is formulated as:

$$D\left(\mathbf{p}|\,\boldsymbol{\alpha}\right)=\begin{cases}\frac{1}{B(\boldsymbol{\alpha})}\Pi_{i=1}^{K}p_i^{\alpha_i-1} & \mathbf{p}\in\mathcal{S}_K\\ 0 & otherwise\end{cases}\tag{1}$$

where $\alpha_i$ is Dirichlet parameter of the $i$-th class. $B\left(\cdot\right)$ is the beta function, and $\mathcal{S}_K=\{\mathbf{p}|\sum_i p_i=1,0\leq p_i\leq 1\}$ is the $K-1$ dimensional unit simplex. In DST, parameter $\alpha_i$ is linked to the class evidence $e_i$, $\alpha_i=e_i+1$, which represents the degree of support for one subject diagnosed as the specific type of liver cancer. Traditional classification model outputs a single point $\mathbf{p}$ in the simplex $\mathcal{S}_K$, while DST quantifies the probability of each point. By probability integral, DST enables to obtain the mean class probability $\hat{p}_i$ and the overall confidence of classification.

In our implementation, we replace the activation function of the last layer with ReLU function and treat the negative output as class evidence $\mathbf{e}$. The uncertainty $u$ and belief masses $b_i$ are derived in terms of subjective logic:

$$u=\frac{K}{S},b_i=\frac{e_i}{S}\tag{2}$$

where $S$ is Dirichlet strength, $S=\sum_{i=1}^{K}\alpha_i$. Belief masses $b_i$ measures the support of $i$-th class and the $K+1$ masses sum to 1, $\sum_{i=1}^{K}b_i+u=1$. We can see that the less total evidence collected indicates the higher uncertainty of prediction. The mean class probability $\hat{p}_i$ can be efficiently computed as $\hat{p}_i=\frac{\alpha_i}{S}$.

**Split of Credible/Incredible Views (SpV)** In DST, pair-wise combination process tends to believe the higher confident view even when they conflict with other views, thus yielding counter-intuitive results. To address this issue, we propose to split input views into credible and incredible views and assess their correlation with the reward and penalty function, respectively.

Specifically, we first calculate the average distance of each view in relation to the others. For $i$-th view, its distance to $j$-th view is calculated by the meaning class probability $\hat{\mathbf{p}}_i$, $d_{ij}=\sqrt{\frac{1}{2}(\hat{\mathbf{p}}_i-\hat{\mathbf{p}}_j)^T(\hat{\mathbf{p}}_i-\hat{\mathbf{p}}_j)}$. Its average value $d_i=\frac{1}{M-1}\sum_{j\neq i}d_{ij}$ measures the degree semantic consistency with other views. The lower $d_i$ means more support from the remaining views, while the larger value indicates for a conflicting or unreliable view. To split the credible and incredible views, we further calculate the semantic consistency threshold $\theta$, $\theta=\frac{1}{M}\sum_i d_i$, where $M$ is the number of input views. When the average distance $d_i$ exceeds the threshold $\theta$, the view is considered to be incredible, otherwise, it is deemed to be credible.

**Reliable Fusion with Correlation Assessment** With the split of credible/incredible views, we introduce the reward and penalty function $f_r\left(f_p\right)$ to calculate the correlation weights $w_i$ in combination with the view uncertainty $u_i$. The two types of functions are defined as:

$$f_r\left(V_i\right)=e^{-\bar{u}_i},V_i\in V_{credible}\tag{3}$$

$$f_p(V_i) = e^{-(1+\bar{u}_{\max}-\bar{u}_i)}, V_i \in V_{incredible} \tag{4}$$

where $\bar{u}_i$ is normalized uncertainty, $\bar{u}_i = u_i / \sum_i u_i$. For the credible view, the lower uncertainty score deserves a larger weight for evidence accumulation. Conversely, for the incredible view, the lower uncertainty results in a smaller weight. Furthermore, we smooth the correlation weight $w_i$ as $w_i' = e^{w_i/\eta} / \sum_{i=1}^{M} e^{w_i/\eta}$, where $\eta$ is temperature factor that adjusts the sensitivity to correlation variance. Finally, we implement the reliable fusion at an evidence level, $\mathbf{e}_f = \sum_i w'_i \mathbf{e}_i$. Based on $\mathbf{e}_f$, we could obtain the mean class probability $\hat{\mathbf{p}}_f$ and the overall uncertainty of multi-view prediction $u_f$.

**Loss Function:** Since the distribution of class probability $\mathbf{p}$ is modeled in DST, classification loss $\mathcal{L}_{cls}$ is formulated as the integral of traditional cross-entropy loss. Additionally, we add a prior constraint by Kullback-Leibler divergence $\mathcal{L}_{kl}$ to enforce incorrect labels to be assigned with few evidence near to zero, $\mathcal{L} = \frac{1}{N} \sum_i \mathcal{L}_{cls}(\alpha_i) + \mathcal{L}_{kl}(\alpha_i)$

$$\begin{aligned} \mathcal{L}_{cls}(\alpha_i) &= \int \left[ \sum\nolimits_{j=1}^{K} -y_{ij} \log p_{ij} \right] \frac{1}{B(\alpha_i)} \Pi_{j=1}^{K} p_{ij}^{\alpha_{ij}-1} dp_i \\ &= y_{ij} \left( \phi(S_i) - \phi(\alpha_{ij}) \right) \end{aligned} \tag{5}$$

$$\begin{aligned} L_{kl}(\alpha_i) &= KL\left[ D(p_i|\tilde{\alpha}_i) \| D(p_i|\mathbf{1}) \right] \\ &= \log\left( \frac{\Gamma\left(\sum_j \tilde{\alpha}_{ij}\right)}{\Gamma(K) \Pi_{j=1}^{K} (\tilde{\alpha}_{ij})} \right) + \sum\nolimits_j (\tilde{\alpha}_{ij} - 1) \left[ \phi(\tilde{\alpha}_{ij}) - \phi\left( \sum\nolimits_j \tilde{\alpha}_{ij} \right) \right] \end{aligned} \tag{6}$$

where $\mathrm{x}_n^i$ denotes the $i$-th CEUS view of $n$-th subject and $y_n$ is the true label of liver cancer. $\phi(\cdot)$ is the digamma function and $\Gamma(\cdot)$ is Gamma function. $y_{ij}$ is the $j$-th element of the onehot class vector $y_i$. $\tilde{\alpha}_i = y_i + (1 - y_i) \odot \alpha_i$ is adjusted parameter which avoids pushing Dirichlet parameter of true class to 1. Our method was trained with Adam optimizer (batchsize: 35, learning rate: 0.0003). The maximal number of training epoch is 1000 and the temperature factor $\eta$ is 0.99.

## 3 Experiments

**Experimental Setup** The whole dataset was split into the training and testing set (ratio: 4:1) by preserving the class percentage. As random partition is involved, we repeated the procedure for 10 times and reported the mean and standard derivation (std.) of testing results. Classification performance was evaluated by classification accuracy (ACC), area under curve (AUC), specificity (SPE), sensitivity (SEN), F1-score and Matthews correlation coefficient (MCC). HCC is labeled as positive class. For each split, we conducted a 5-fold cross-validation on the training set for hyper-parameters search.

**Table 1.** Comparison of state-of-the-art methods. Results are presented in form of [Mean±Std]%.

| Method | ACC | AUC | SPE | SEN | F1-score | MCC |
|---|---|---|---|---|---|---|
| GCCA | 76.67±6.50 | 72.29±8.84 | 88.94±8.06 | 57.65±17.51 | 64.94±13.36 | 51.00±12.92 |
| KCCA | 77.29±5.15 | 77.40±9.72 | 82.28±6.15 | 68.46±16.22 | 69.45±13.12 | 51.28±14.12 |
| DCCA | 80.63±3.68 | 83.81±5.08 | 85.71±6.71 | 74.15±8.44 | 75.17±5.17 | 60.25±7.27 |
| TMC | 86.67±3.70 | 86.90±3.63 | 90.12±3.94 | 81.70±7.53 | 83.08±3.90 | 72.25±6.93 |
| ETMC | 88.13±2.95 | 87.68±4.24 | 91.67±3.97 | **83.38±8.05** | 84.82±3.44 | 75.49±5.88 |
| QMF | 84.58±3.83 | 86.04±4.03 | 91.42±5.30 | 75.16±8.16 | 79.52±4.80 | 68.19±7.01 |
| CAMVF(Ours) | 88.13±3.68 | 88.24±4.67 | **92.55±4.94** | 81.42±6.26 | 84.57±4.49 | 75.17±7.44 |
| ECAMVF(Ours) | **88.33±1.76** | **88.29±3.14** | 92.48±3.39 | 82.95±6.59 | **84.99±1.69** | **75.94±2.97** |

The competing methods include Canonical Correlation Analysis (CCA) based multi-view learning methods, i.e., Generalized CCA (**GCCA**)[1], Kernel CCA (**KCCA**)[13], and Deep CCA (**DCCA**)[2], and the state-of-the-art trusted multi-view classification (TMC) methods, i.e., **TMC**[10], enhanced TMC (**ETMC**)[10] and Quality-aware multi-modality fusion (**QMF**))[19]. Among which, ETMC was implemented by adding a mixed view that concatenated all view representations, aiming to complement view interaction at the feature level not limited to the decision layer. Similarly, we also added the same mixed view to our CAMVF method, i.e., enhanced CAMVF (**ECAMVF**). For a fair comparison, these competing methods were implemented with the same backbone as our method for view feature extraction.

**Diagnostic Performance:** From the Table 1, we have the following three observations. First, trusted multi-view learning methods (i.e., TMC, QMF, and our CAMVF, etc.) achieve better classification results than various CCA variants, with the ACC and AUC exceeding 84% and 86%, respectively. Among which, our method CAMVF(ECAMVF) achieve the best performance with an ACC of 88.13%(88.33%) and AUC of 88.24%(88.29%). This shows that, dynamically assessing view correlation is effective to multi-view CEUS fusion for PLC diagnosis, and assigning all views with equal importance would lead to inferior performance biased by the incredible views. Second, our CAMVF (ECAMVF) method consistently outperform the TMC as well as its enhanced version ETMC in terms of ACC, AUC and SPE, etc. The ETMC method slightly outperforms our ECAMVF method with p-value $> 0.8$ in terms of SEN. It validates the superiority of credible/incredible view identification for the possible conflict view combination against Dempster's rule. Third, we find that the specificity scores of various methods are significantly higher than the sensitivity scores, demonstrating that HCC is easier to be falsely classified as ICC. It is perhaps due to that the diversity of enhancement pattern of HCC is higher than that of ICC, and enhancement patterns of HCC overlap with those of ICC partially.

**Table 2.** Results of ablation experimentspresented in form of [Mean±Std]%.

| Method | EvU | SpV | Mixed view | ACC | AUC | F1-score | MCC |
|---|---|---|---|---|---|---|---|
| Ensemble-major | - | - | - | 82.29±6.75 | 82.48±6.08 | 74.75±7.46 | 64.18±12.09 |
| Evi-mean | ✓ | - | - | 87.08±3.37 | 87.79±3.55 | 83.55±3.66 | 73.26±6.35 |
| Evi-uncertainty | ✓ | - | - | 86.46±3.44 | 87.22±3.16 | 82.56±4.11 | 72.02±6.73 |
| CAMVF(Ours) | ✓ | ✓ | - | 88.13±3.68 | 88.24±4.67 | 84.57±4.49 | 75.17±7.44 |
| ECAMVF(Ours) | ✓ | ✓ | ✓ | **88.33±1.76** | **88.29±3.14** | **84.99±1.69** | **75.94±2.97** |

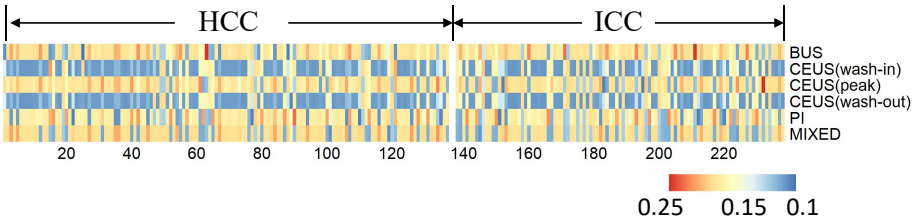


**Fig. 2.** Visualization of CEUS view correlation for PLC differential diagnosis.

**Ablation Experiments** To evaluate the contributions of two major components of our method (i.e., evidence-based uncertainty (EvU) and split of credible/incredible views (SpV)), we compare CAMVF with its three variants. The first variant **Ensemble-major** removes the EvU and SpV modules and ensembles view predictions by the majority vote mechanism. The second variant **Evi-mean** combines view evidence with the equal importance weight and the third variant **Evi-uncertainty** assesses view importance weights with the uncertainty score only without the split of credible/incredible views. Results are presented in Table 2.

We could have at least three observations. First, our method consistently yields better results than three variants. For example, the ACC and AUC scores of three variants are both below 88%, and F1-score and MCC are below 84% and 74%, respectively. It validates the effectiveness of dynamic fusion with correlation assessment for multi-view CEUS classification. Second, we find that combining CEUS views at the evidence level (both for Evidence-mean and -uncertainty) consistently outperform label-level ensemble method Ensemble-major, which implies that fusing CEUS views at an evidence level is an indispensable step for performance improvement. Additionally, it provides prediction confidence estimation for high-stakes PLC diagnosis. Third, two evidence-based fusion method achieve the limited performance with ACC of 86% and AUC of 87%. This demonstrates that the split of credible/incredible view is important in case of conflict views, and assigning a much smaller weight to incredible view could avoid their wrong guidance.

**Visualization of View Correlation** To display the learned view correlation in a more intuitive manner, we plotted the color map of correlation matrix (Fig. 2). We can see that CEUS frames either in wash-in or wash-out stages with the half peak intensity deserve the lower diagnostic correlation than other views. And BUS and CEUS peak frames consistently have higher correlation than PI and mixed view. In addition, we find that ICC cases show slightly higher view correlation variances than that of HCC, i.e., less color changes across subjects. It suggests that radiologists should pay more attention to identify valuable findings across various views for ICC cases.

## 4 Conclusion

In this paper, we have proposed a correlation-adaptive multi-view fusion method for dual-screen CEUS based liver cancer diagnosis. Experimental results have demonstrated the effectiveness of our method in the identification of credible view according to the varying correlation for PLC diagnosis, especially for dealing with conflict views. As the future work, we will extend the current model with a novel view evidence collection module that replaces the pure neural network with a well-explained mechanism.

**Acknowledgments.** This work was funded in part by the Jiangsu Funding Program for Excellent Postdoctoral Talent (No. 2024ZB020), Postdoctoral Fellowship Program of CPSF (No. GZC20242233), National Natural Science Foundation of China (No. 62136004, 62276130, 62272226), the National Key R&D Program of China (No. 2023YFF1204803), the Key Research and Development Plan of Jiangsu Province (No. BE2022842, BE2022677), Clinical Trials from the Affiliated Drum Tower Hospital, Medical School of Nanjing University(2022-LCYJ-MS-24, 2022-YXZX-YX-08).

**Disclosure of Interests.** The authors have no competing interests to declare that are relevant to the content of this article.

## References

1. Afshin-Pour, B., Hossein-Zadeh, G.A., Strother, S.C., Soltanian-Zadeh, H.: Enhancing reproducibility of fmri statistical maps using generalized canonical correlation analysis in npairs framework. NeuroImage **60**(4), 1970–1981 (2012)
2. Andrew, G., Arora, R., Bilmes, J., Livescu, K.: Deep canonical correlation analysis. In: International Conference on Machine Learning. pp. 1247–1255. PMLR (2013)
3. Atrey, P.K., Hossain, M.A., El Saddik, A., Kankanhalli, M.S.: Multimodal fusion for multimedia analysis: a survey. Multimedia Systems **16**, 345–379 (2010)
4. Barr, R.G., Huang, P., Luo, Y., Xie, X., Zheng, R., Yan, K., Jing, X., Luo, Y., Xu, H., Fei, X., et al.: Contrast-enhanced ultrasound imaging of the liver: a review of the clinical evidence for sonovue and sonazoid. Abdominal Radiology **45**, 3779–3788 (2020)
5. D'Onofrio, M., Crosara, S., De Robertis, R., Canestrini, S., Mucelli, R.P.: Contrast-enhanced ultrasound of focal liver lesions. American Journal of Roentgenology **205**(1), W56–W66 (2015)

6. Feng, M., Pan, Y., Kong, R., Shu, S.: Therapy of primary liver cancer. The Innovation **1**(2) (2020)
7. Feng, X., Cai, W., Zheng, R., Tang, L., Zhou, J., Wang, H., Liao, J., Luo, B., Cheng, W., Wei, A., et al.: Diagnosis of hepatocellular carcinoma using deep network with multi-view enhanced patterns mined in contrast-enhanced ultrasound data. Engineering Applications of Artificial Intelligence **118**, 105635 (2023)
8. Guo, L.H., Wang, D., Qian, Y.Y., Zheng, X., Zhao, C.K., Li, X.L., Bo, X.W., Yue, W.W., Zhang, Q., Shi, J., et al.: A two-stage multi-view learning framework based computer-aided diagnosis of liver tumors with contrast enhanced ultrasound images. Clinical Hemorheology and Microcirculation **69**(3), 343–354 (2018)
9. Guo, L., Wang, D., Xu, H., Qian, Y., Wang, C., Zheng, X., Zhang, Q., Shi, J.: Ceus-based classification of liver tumors with deep canonical correlation analysis and multi-kernel learning. In: 2017 39th Annual International Conference of the IEEE Engineering in Medicine and Biology Society (EMBC). pp. 1748–1751 (2017)
10. Han, Z., Zhang, C., Fu, H., Zhou, J.T.: Trusted multi-view classification with dynamic evidential fusion. IEEE Transactions on Pattern Analysis and Machine Intelligence **45**(2), 2551–2566 (2022)
11. Jiang, W., Xie, C., Wei, B., Zhou, D.: A modified method for risk evaluation in failure modes and effects analysis of aircraft turbine rotor blades. Advances in Mechanical Engineering **8**(4), 1687814016644579 (2016)
12. Jiang, X., Wang, J., Deng, X., Xiong, F., Zhang, S., Gong, Z., Li, X., Cao, K., Deng, H., He, Y., et al.: The role of microenvironment in tumor angiogenesis. Journal of Experimental & Clinical Cancer Research **39**(1), 1–19 (2020)
13. Kuss, M., Graepel, T.: The geometry of kernel canonical correlation analysis (2003)
14. Liu, W., Yue, X., Chen, Y., Denoeux, T.: Trusted multi-view deep learning with opinion aggregation. In: Proceedings of the AAAI Conference on Artificial Intelligence. vol. 36, pp. 7585–7593 (2022)
15. Pérez-Rúa, J.M., Vielzeuf, V., Pateux, S., Baccouche, M., Jurie, F.: Mfas: Multimodal fusion architecture search. In: Proceedings of the IEEE/CVF Conference on Computer Vision and Pattern Recognition. pp. 6966–6975 (2019)
16. Shafer, G.: Dempster-shafer theory. Encyclopedia of Artificial Intelligence **1**, 330–331 (1992)
17. Sung, H., Ferlay, J., Siegel, R.L., Laversanne, M., Soerjomataram, I., Jemal, A., Bray, F.: Global cancer statistics 2020: GLOBOCAN estimates of incidence and mortality worldwide for 36 cancers in 185 countries. CA: A Cancer Journal for Clinicians **71**(3), 209–249 (2021)
18. Wang, K., Zhang, H., Xia, Y., Liu, J., Shen, F.: Surgical options for intrahepatic cholangiocarcinoma. Hepatobiliary Surgery and Nutrition **6**(2), 79 (2017)
19. Zhang, Q., Wu, H., Zhang, C., Hu, Q., Fu, H., Zhou, J.T., Peng, X.: Provable dynamic fusion for low-quality multimodal data. arXiv preprint arXiv:2306.02050 (2023)
20. Zou, K., Yuan, X., Shen, X., Wang, M., Fu, H.: Tbrats: Trusted brain tumor segmentation. In: International Conference on Medical Image Computing and Computer-Assisted Intervention. pp. 503–513. Springer (2022)
21. Zwanenburg, A., Vallières, M., Abdalah, M.A., Aerts, H.J., Andrearczyk, V., Apte, A., Ashrafinia, S., Bakas, S., Beukinga, R.J., Boellaard, R., et al.: The image biomarker standardization initiative: standardized quantitative radiomics for high-throughput image-based phenotyping. Radiology **295**(2), 328–338 (2020)